Self-organization of an acentrosomal microtubule network at the basal cortex of polarized epithelial cells

Amy Reilein, Soichiro Yamada, and W. James Nelson

Department of Biological Sciences and Department of Molecular and Cellular Physiology, Beckman Center for Molecular and Genetic Medicine, Stanford University School of Medicine, Stanford, CA 94305

Mechanisms underlying the organization of centrosome-derived microtubule arrays are well understood, but less is known about how acentrosomal microtubule networks are formed. The basal cortex of polarized epithelial cells contains a microtubule network of mixed polarity. We examined how this network is organized by imaging microtubule dynamics in acentrosomal basal cytoplasts derived from these cells. We show that the steady-state microtubule network appears to form by a combination of microtubule–microtubule and microtubule–cortex interactions, both of which increase microtubule stability. We used computational modeling to determine whether these microtubule parameters are sufficient to generate a steady-state acentrosomal microtubule network. Microtubules undergoing dynamic instability without any stabilization points continuously remodel their organization without reaching a steady-state network. However, the addition of increased microtubule stabilization at microtubule–microtubule and microtubule–cortex interactions results in the rapid assembly of a steady-state microtubule network in silico that is remarkably similar to networks formed in situ. These results define minimal parameters for the self-organization of an acentrosomal microtubule network.

Introduction

The classic conceptual framework for considering how microtubule organization is regulated is based on studies of cells in which the centrosome nucleates and organizes cytoplasmic microtubules. In this case, microtubule minus ends are located at or around the centrosome, and dynamic plus ends undergo cycles of growth and shrinkage, which is termed dynamic instability (Mitchison and Kirschner, 1984), as they probe the cell periphery. However, other types of microtubule organizations are also formed in the absence of centrosomes, including microtubule bundles, arrays, and networks (for review see Keating and Borisy, 1999). This raises the question as to how these acentrosomal networks are formed. Radial arrays can be organized by the minus end–directed microtubule motor dynein on the surface of pigment granules (Vorobjev et al., 2001; Cytrynbaum et al., 2004; Malikov et al., 2004) or by a combination of plus and minus end–directed motors (Sawin et al., 1992; Nedelec et al., 1997; Surrey et al., 2001). Plant cortical microtubules become organized into bundles through initial contacts between microtubules undergoing dynamic instability followed by lateral zippering and completion of bundling through microtubule treadmilling (Shaw et al., 2003; Dixit and Cyr, 2004a,b). A web-like network of microtubules of mixed polarity is present on the basal membrane of polarized epithelial cells (Bre et al., 1987; Bacallao et al., 1989; Gilbert et al., 1991), which is a site for endocytosis and transcytosis of vesicles (Perret et al., 2005). The origin and mechanism of organization of this acentrosomal network in polarized epithelial cells are not understood.

Microtubules in epithelial cells have properties that distinguish them from microtubules in fibroblastic-like cells (Pepperkok et al., 1990; Shelden and Wadsworth, 1993; Waterman-Storer et al., 2000). The rates of growth and shortening are slower, the length of growth and shortening events is shorter, microtubule dynamicity (the total length grown and shortened divided by the life span of the microtubule) is lower (Shelden and Wadsworth, 1993), and cadherin-mediated cell–cell contact leads to microtubule stabilization (Chausovsky et al., 2000). Acentrosomal microtubules can arise spontaneously in the peripheral cytoplasm and persist for many minutes; the

A. Reilein and S. Yamada contributed equally to this paper.

Correspondence to W. James Nelson: wjnelson@stanford.edu

A. Reilein's current address is Margaret M. Dyson Vision Research Institute, Weill Medical College of Cornell University, New York, NY 10021.

Abbreviations used in this paper: APC, adenomatous polyposis coli protein; EB1, end-binding protein 1; td, tandem dimer.

The online version of this article contains supplemental material.

The Journal of Cell Biology, Vol. 171, No. 5, December 5, 2005 845–855
http://www.jcb.org/cgi/doi/10.1083/jcb.200505071

minus ends of these microtubules are quite stable (Vorobjev et al., 1997; Yvon and Wadsworth, 1997). Microtubules in cytoplasts (acentrosomal enucleated cells) derived from epithelial cells display dynamic instability but not the treadmilling behavior observed in fibroblast-derived cytoplasts, supporting the idea that in epithelial cells, the minus end of microtubules is stable to depolymerization (Rodionov et al., 1999). It is not known whether these or other microtubule parameters contribute to the unique acentrosomal organization of microtubule networks in polarized epithelial cells.

To examine this problem, we studied microtubules on basal plasma membranes isolated from fully polarized MDCK epithelial cells. These basal membranes allow us to observe microtubule networks that are associated with the plasma membrane in considerably more detail than is possible in an intact cell. We have found that microtubules in basal membrane cytoplasts have an organization and dynamics that are similar to microtubules in intact MDCK cells and transport endocytic vesicles at rates consistent with motor-driven transport. Previously, we showed that the +Tip proteins APC (adenomatous polyposis coli protein), EB1 (end-binding protein 1), and $p150^{Glued}$ are distributed along these microtubules and that APC bound to the basal cortex acts as a template for microtubule binding and polymerization (Reilein and Nelson, 2005). In this study, we examine microtubule dynamics in detail and show how microtubule interactions with one another and the underlying cortex can generate a steady-state network in situ and in silico that has characteristics of a self-organized structure.

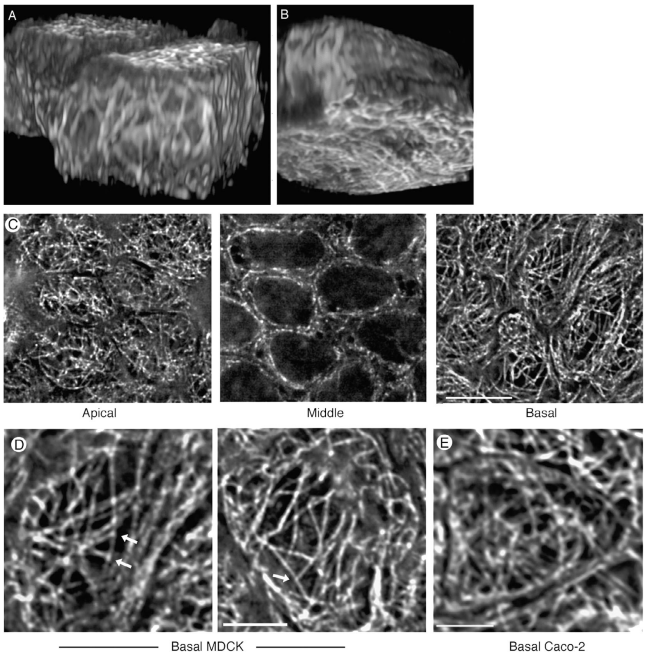

Figure 1. **Microtubule organization in polarized epithelial cells shows microtubule–microtubules intersections in the basal network.** (A) GFP-tubulin–expressing MDCK cells reconstructed from images spaced 0.2 μm apart in the z axis. (B) Image rotated with Volocity software to provide a view looking from the bottom of the cells upwards to show the microtubule network on the basal surface. (C) Deconvolution microscopy of tubulin immunofluorescence at representative basal, middle, and apical sections of polarized MDCK cells shows the webbed microtubule network apical and basal to the nucleus and microtubule bundles running alongside the nucleus parallel to the lateral membrane. Bar, 10 μm. (D) Close-up views of the basal network of individual cells show intersections formed by microtubules (arrows) and the variable weave of the microtubule network. (E) Microtubules at the base of a Caco-2 cell are organized into a similar intersecting network. (D and E) Bars, 5 μm.

Results

Microtubules form an integrated network on the basal membrane of polarized epithelial cells

Microtubules in columnar epithelial cells are organized in the apico–basal axis of the cell into parallel bundles with their plus ends oriented toward the basal membrane and weblike networks on the apical and basal cortex (Fig. 1, A–C; Bacallao et al., 1989; Gilbert et al., 1991; Meads and Schroer, 1995; Eaton et al., 1996). High resolution imaging of microtubules on the basal cortex reveals a network of microtubules formed by intersections that arise from the termination of one microtubule on the side of another or from two microtubules crossing over one another (Fig. 1, D and E). A similar microtubule network is found on the basal cortex of different types of polarized epithelial cells, including Caco-2 cells derived from colonic epithelium (Figs. 1 E and 2 D) and EpH4 cells derived from mammary epithelium (Fig. 2 E).

Microtubule organization on basal membrane patches

Because of the high density and complex organization of microtubules and the columnar shape of polarized epithelial cells, monitoring individual microtubule dynamics in intact cells is technically challenging. Therefore, we isolated basal membranes and the associated cytoskeleton from fully polarized MDCK epithelial cells on filters by hypotonic swelling and sonication (Heuser, 2000). The reduced number of microtubules in these basal patches allowed us to identify microtubule distributions and activities that contribute to the organization of these basal microtubule networks. Microtubules remain attached to isolated basal membrane patches in an interwoven, branched network that is identical in appearance to that in intact cells (compare Figs. 1 D with 2 A). Some membrane patches form cytoplasts, presumably because residual lateral membranes anneal over the top of the basal membrane (Fig. 2 B); the distribution and dynamics of microtubules in these isolated cortical cytoplasts are similar to those of microtubules on open basal patches and in intact cells (see Microtubule dynamics....network).

Immunofluorescence and scanning electron microscopy revealed that the basal microtubule network is organized by microtubules intersecting one another at a range of angles and often involves the convergence of multiple microtubules (Fig. 2). This organization is common to polarized MDCK, Caco-2, and EpH4 epithelial cells (Fig. 2, C–E). Microtubule ends contacting the sides of other microtubules have different conformations (Fig. 2, F–I), sometimes curving at the tip and sometimes terminating in a bulge or knob. Microtubules are often curved or looped (Fig. 2, C, D, G, and K). Regularly spaced disconti-

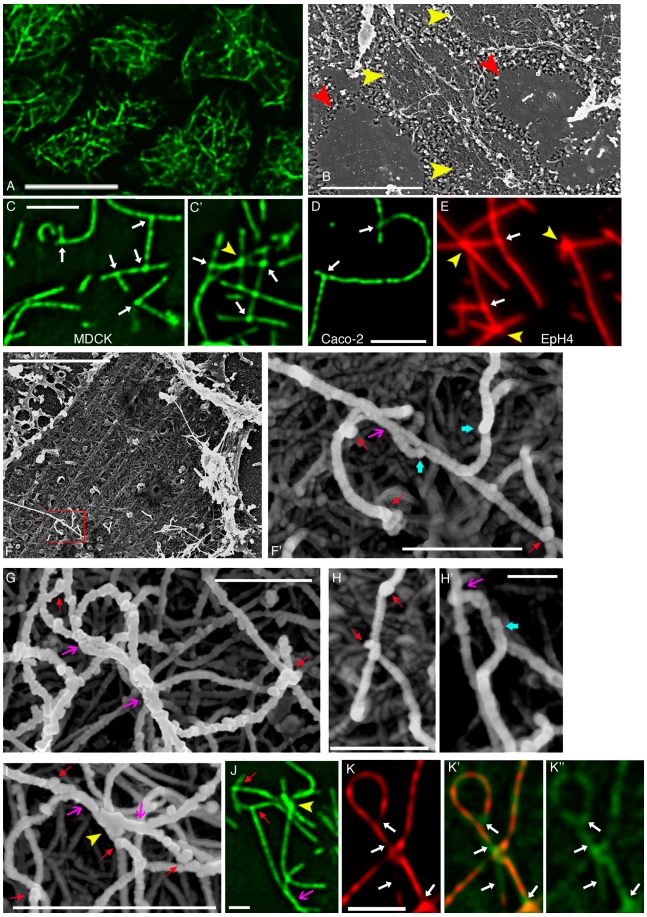

Figure 2. **Microtubules are arranged into intersecting networks on isolated basal membrane patches.** (A) GFP-tubulin–labeled microtubules on basal membrane patches prepared from MDCK cells that were polarized on filters. (B) Scanning electron microscopy of MDCK cell basal patches shows cytoplasts (red arrowheads) and open patches (yellow arrowheads). (A and B) Bars, 10 μm. (C) Two examples of GFP-labeled microtubules on MDCK basal patches show the presence of microtubule–microtubule intersections (arrows) and the intersection of multiple microtubules at a focus (yellow arrowhead). (D) Immunofluorescence staining of microtubules on the basal membrane isolated from a polarized Caco-2 cell shows the presence of end-to-side microtubule intersections (arrows). (C and D) Bars, 2.5 μm. (E) An isolated basal membrane from an EpH4 cell shows the presence of a microtubule network with intersections (arrows). Multiple microtubules often intersect at one focus (arrowheads). (F) Scanning electron microscopy of a basal patch shows a few microtubules that remain (boxed and enlarged at right) overlying a dense cytoskeletal network containing actin stress fibers (the microtubules are brighter because they scatter more secondary electrons with their exposed edges). Bar (left), 5 μm. Microtubule ends terminate on the sides of other microtubules and exhibit different conformations. Red arrows point to enlarged ends of microtubules; blue arrows point to ends that curve as they terminate on the sides on other microtubules. Microtubules also show side-to-side interactions (pink arrow). Bar (right), 0.5 μm. (G) Gold labeling of the microtubule network. Microtubules are densely coated with gold beads along their length. Microtubule ends terminate on the sides of other microtubules (red arrows). Microtubules also bundle (pink arrows). Bar, 0.5 μm. (H) Additional examples of the different conformations of microtubule ends contacting the sides of other microtubules. Enlargements present at the end of microtubules are shown by red arrows. Bar (left), 0.5 μm. An end without an enlargement is shown by the blue arrow. Bar (right), 200 nm. A side-to-side interaction is indicated by the pink arrow. (I) Multiple microtubules converging at a focus (yellow arrowhead) and exhibiting end-to-side interactions (red arrows) and side-to-side interactions (pink arrows). Bar, 0.5 μm. (J) GFP-tubulin–labeled microtubules on a nonfixed MDCK basal patch show that the appearance of the intersections is not a result of fixation (arrows). The yellow arrowhead indicates a focus of microtubules; red arrows show end-to-side microtubule intersections; pink arrow shows a side-to-side microtubule interaction. Bar, 1 μm. (K) Tubulin antibody staining (red; left) of GFP-labeled microtubules (far right) shows that GFP fluorescence shows through areas of diminished antibody staining (arrows; merged image in middle). Bar, 2.5 μm.

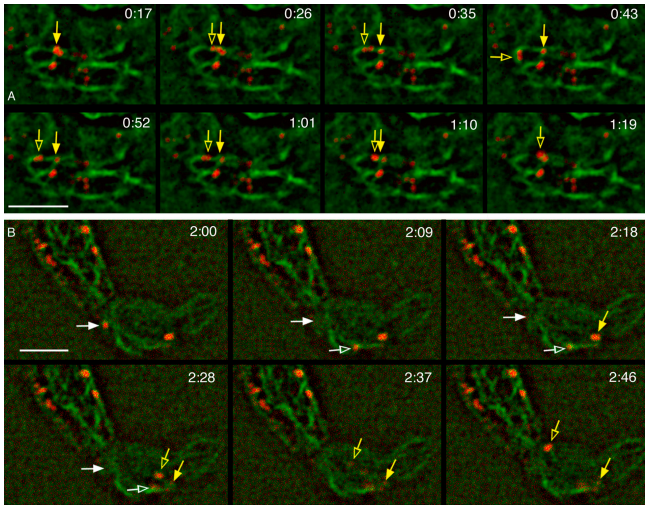

Figure 3. **Basal microtubules transport endocytic vesicles.** Closed arrows denote initial vesicle positions, and open arrows indicate current locations of vesicles. (A) A basal cytoplast isolated from polarized GFP-tubulin–expressing MDCK cells that had been incubated with LysoTracker red (Video 1, available at http://www.jcb.org/cgi/content/full/jcb.200505071/DC1). (B) A basal cytoplast isolated from polarized cells expressing clathrin light chain–DsRed (Video 2). The yellow and white arrows show two examples of vesicles that move on microtubules. Bars, 5 μm.

nuities of reduced fluorescence are observed along microtubules in tubulin antibody-stained as well as GFP-tubulin–labeled microtubules (Fig. 2, C and D). These discontinuities are observed in deconvolved and nondeconvolved images, by confocal microscopy (unpublished data), and in unfixed microtubules containing GFP-tubulin (Fig. 2 J). Note that fixed GFP-tubulin specimens stained with tubulin antibody showed GFP fluorescence in gaps of antibody staining (Fig. 2 K) and vice versa, indicating that the gaps are caused by stearic inhibition of antibody binding or GFP-tubulin fluorescence, which is probably a result of +Tip proteins bound along the length of the microtubules (Reilein and Nelson, 2005).

Basal microtubules serve to transport endocytic vesicles

The basolateral membrane of polarized epithelial cells is a site of endocytosis and transcytosis of internalized vesicles (Perret et al., 2005). To determine whether basal microtubules are functional in endocytic vesicle transport, we prepared basal cytoplasts from polarized cells that had been incubated with LysoTracker red to label acidified vesicles or from cells that had been transfected with clathrin-DsRed to label endocytic vesicles. Both LysoTracker red– (Fig. 3 A and Video 1, available at http://www.jcb.org/cgi/content/full/jcb.200505071/DC1) and clathrin-DsRed–labeled vesicles (Fig. 3 B and Video 2) translocated along basal microtubules at rates ranging from 0.2 to 0.5 μm/s, which is consistent with microtubule motor-driven

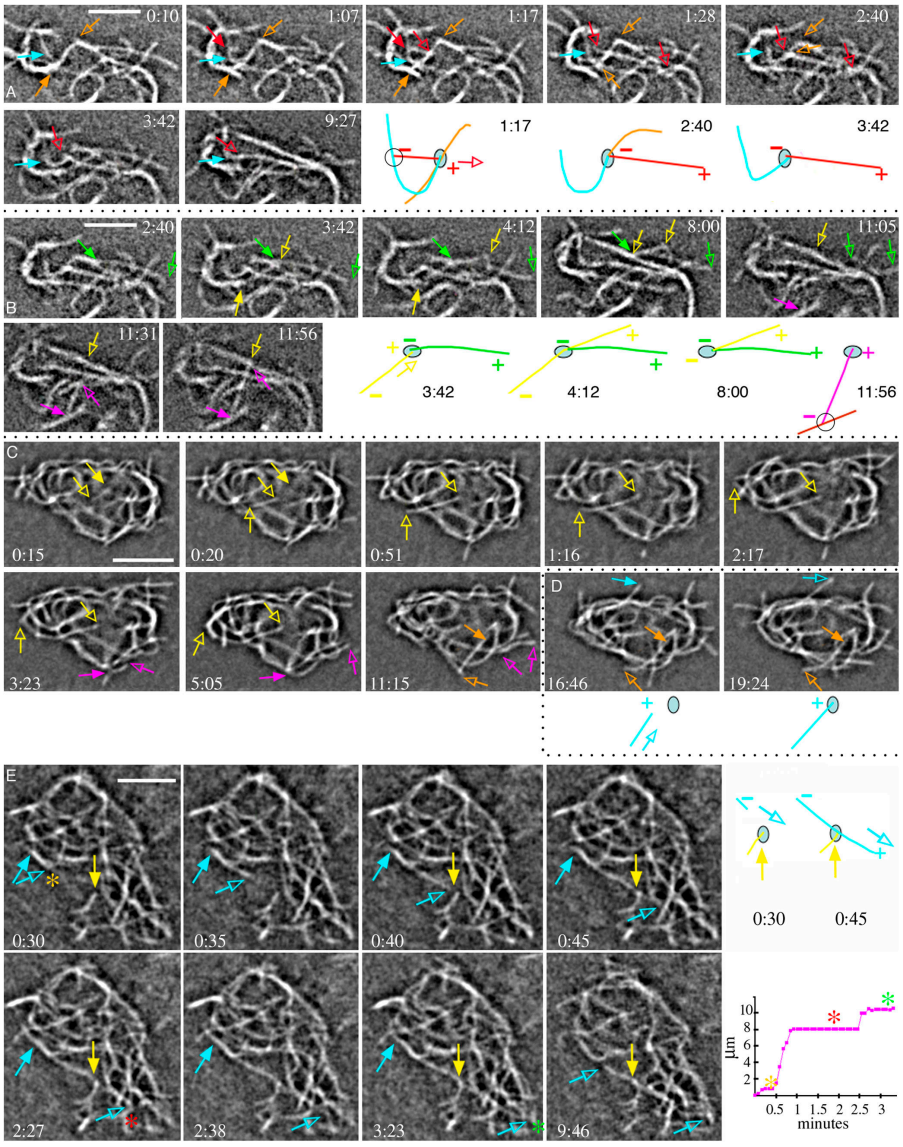

Figure 4. **New microtubules arise and are integrated into the existing network.** Ovals represent points of stabilization on the cortex. Circles indicate the growth of microtubules from the sides of other microtubules. Microtubules are referred to by arrow color. Note that most microtubules grow distances of 5 µm or more. (A) Depolymerization to a fixed location; corresponds to Video 3 (available at http://www.jcb.org/cgi/content/full/jcb.200505071/DC1). The red microtubule arises (red arrow and red line in schematic drawing) apparently from the side of the blue microtubule. After 15 s, the minus end of the red microtubule shrinks to a nearby location that is traversed by the orange microtubule and remains at this location for the 25 min of imaging. The orange microtubule depolymerizes. The end of the blue microtubule has formed a connection with the red microtubule. (B) Growth to a fixed location. The yellow microtubule grows upward to the location where the green microtubule begins and then continues to grow at a different angle. After a few minutes, the yellow microtubule depolymerizes from its minus end and pauses at this same point (see drawing). The green microtubule depolymerizes as well. Later, the pink microtubule arises and grows to this same location (yellow arrow is carried through to mark the location). (C) Depolymerization to a fixed location; corresponds to Video 4. The yellow arrows show a microtubule that arises and whose minus end quickly shrinks and is stabilized nearby. This microtubule curves as it grows, interacts with other microtubules, and remains in the network for the 23 min of imaging. The pink microtubule arises and, after 7 min, depolymerizes from its minus end, pausing at points on the cortex and at another microtubule during depolymerization. The orange microtubule arises and persists for the duration of imaging (15 min). (D) Stabilization of the plus end at a fixed location. The light blue microtubule grows to and becomes stabilized at a point on the basal cortex (see drawing). (E) Growth over a fixed location; corresponds to Video 5. The blue microtubule grows over the same point (yellow arrow) where another microtubule ends and interacts with this microtubule (it bends slightly). The plus end of the blue microtubule continues to grow, pausing at different microtubules along its path (bottom, open arrows; see life history plot to the right; asterisks indicate points of pause). At the end of imaging, the minus end of the blue microtubule has depolymerized a short distance and becomes stabilized at a point along its path (last panel). The microtubule had paused at this same location while growing. Bars, 5 µm.

activities. To quantify the percentage of vesicles that moved, we considered only those patches in which some vesicles moved to be sure that they were active and had sealed over to form cytoplasts. We counted vesicles that moved at least 1.3 µm in directed lateral movements over a period of 1 min and found that 21% of LysoTracker red–labeled vesicles (24/114 vesicles in 11 basal cytoplasts) exhibited directed lateral movement. The percentage of clathrin vesicles moving was more difficult to determine because of the lower intensity of some clathrin-DsRed spots. However, an approximate estimate showed that 7–20% of clathrin spots moved per minute. Note that it has been reported that in whole cells imaged by total internal reflection fluorescence microscopy, only 2% of clathrin spots moved laterally per minute at rates of microtubule motors in CHO cells (Rappoport et al., 2003), and 7% moved in CV-1 cells (Keyel et al., 2004). We conclude that the microtubule network in basal cytoplasts from polarized MDCK cells is functional in the transport of acidified and clathrin-containing endocytic vesicles.

Microtubule dynamics contributing to the organization of the microtubule network

Microtubule dynamics were directly imaged in basal membrane cytoplasts that were prepared from polarized MDCK cells expressing GFP-tubulin. The majority of basal cytoplasts contained a steady-state network of microtubules in which the overall dimensions and organization of microtubules remained stable (Fig. 4). Generally, the network consists of many short (5.2 ± 2.2 µm) microtubules that arrange themselves into a network as they encounter one another through growth and shrinkage and form connections by adhering to one another end-to-side and side-to-side. Microtubules also bind to the

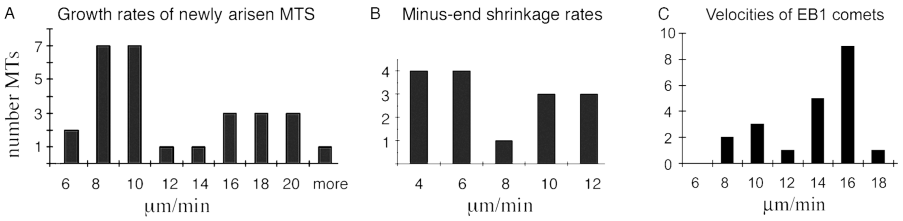

Figure 5. **Microtubules grow and shrink at a wide distribution of rates.** (A) Bimodal distribution of growth rates of new microtubules that arise on basal membrane patches. (B) Distribution of minus end shrinkage rates of newly arisen microtubules. (C) Distribution of growth rates of new microtubules marked by EB1-td DsRed.

basal cortex (Reilein and Nelson, 2005). The striking feature of the basal microtubule network is that it appears to be organized predominantly by stable interactions between individual microtubules and between microtubules and the basal cortex. Note, however, that the network is also undergoing slow, subtle remodeling by dynamic instability and de novo growth of a few microtubules.

We next sought to characterize microtubule stability and dynamics within these networks to understand how the network is organized. Most of the cytoplasts exhibited dynamic microtubule growth and shrinkage at the periphery of the cytoplast, although not all of the microtubules were active (see, for example, Fig. 4 E and Video 5, available at http://www.jcb.org/cgi/content/full/jcb.200505071/DC1). The reason for the lack of dynamic instability in some cases is unknown, but it could be a result of the stabilization of microtubule ends. Because microtubules in these patches were arising de novo (Fig. 4 E and Video 5), it is less likely that the lack of dynamics of other microtubules is caused by a low concentration of tubulin dimers. Dynamic instability of existing microtubules at the margins of basal MDCK cytoplasts is characterized by short periods and slow rates of growth (2.54 ± 0.65 μm/min) and shortening (5.06 ± 1.49 μm/min; Table I). These rates are comparable to those found in dense monolayers of newt lung epithelial cells (4.3 ± 3.6 μm/min growth rate and 3.7 ± 2.4 μm/min shortening rate; Waterman-Storer et al., 2000).

New microtubules arose frequently on basal membrane patches and grew over distances of 3–10 μm, which is the width of a typical basal membrane patch. Microtubules appeared to originate from the sides of other microtubules (Fig. 4 and Video 3, available at http://www.jcb.org/cgi/content/full/jcb.200505071/DC1). New microtubules grew much faster than microtubules undergoing dynamic instability at the margins of cytoplasts, with rates that fell into a bimodal distribution (18.06 ± 3.26 μm/min and 7.54 ± 1.24 μm/min; Table I and Fig. 5). These rates are consistent with those measured in nonpolarized MDCK cells (unpublished data) and in other epithelial cell types (Shelden and Wadsworth, 1993; Waterman-Storer et al., 2000). Microtubules either grew over the entire distance at the fast rate, the entire distance at the slower rate, or, in a few cases, at alternating fast and slow rates while traversing different areas of the basal patch (Video 4).

Generally, new microtubules grew without shrinking and did not exhibit dynamic instability until they reached the margin of the cortical patch (Video 4); a similar microtubule behavior was reported in fibroblasts (Komarova et al., 2002). Microtubules often grew over points where other microtubule ends were located (Fig. 4 E and Video 5), indicating that there are points on the cortex or microtubules for microtubule binding and stabilization. We have identified many proteins that decorate the length of microtubules and that are present at microtubule–microtubule and microtubule–cortex intersections, including EB1, $p150^{glued}$, Kap3, and APC; of these proteins, we showed that antibodies to APC can block exogenous microtubule assembly on the patch (Reilein and Nelson, 2005). At present, the identity of proteins that regulate microtubule nucleation on the sides of other microtubules or on the cortex is poorly understood. γ-Tubulin has been shown recently to nucleate microtubule growth on the sides of other microtubules in fungi and plants (Janson et al., 2005; Murata et al., 2005). Microtubule branches arise on the plant cell cortex when γ-tubulin is recruited from the cytoplasm to the side of a microtubule (Murata et al., 2005). Examination of γ-tubulin staining on basal membrane patches showed that γ-tubulin is localized along the length of microtubules, at branch points, and on the cortex independently of microtubules (Fig. 6). Typ-

Table I. **Microtubule dynamics parameters in basal membrane cytoplasts**

Microtubule end	Parameter	Dynamic instability	New microtubules
Plus end	Catastrophe frequency (min^{-1})	0.95	ND
	Rescue frequency (min^{-1})	0.98	ND
Plus end growth	Rate (μm/min)	2.54 ± 0.65 (*n* = 34)	18.06 ± 3.26 (*n* = 10)[a] 7.55 ± 1.24 (*n* = 17)[a]
	Length (μm)	0.79 ± 0.37	6.92 ± 2.44
	Duration (s)	17.3 ± 12.6	ND
Plus end shortening	Rate (μm/min)	5.06 ± 1.49 (*n* = 41)	12.73 ± 6.08 (*n* = 5)
	Length (μm)	0.94 ± 0.36	ND
	Duration (s)	13.2 ± 5.1	ND
Minus end shortening	Rate (μm/min)	NA	7.49 ± 3.36 (*n* = 17)[a]

Values are means ± SD. NA, not applicable.
[a]See Fig. 5.

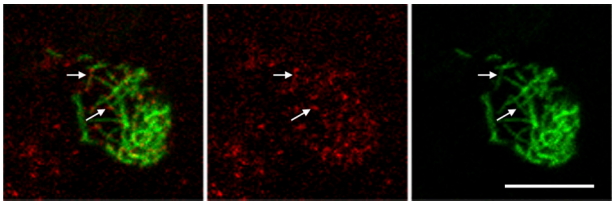

Figure 6. **Localization of γ-tubulin on basal patches.** Basal patches prepared from GFP-tubulin–expressing MDCK cells polarized on filters were stained for γ-tubulin (red). γ-Tubulin is localized along microtubules, at branch points (arrows), and in association with the cortex independently of microtubules. Bar, 5 μm.

ical centrosomal staining by the γ-tubulin antibody as well as noncentrosomal staining was observed in intact MDCK cells (Fig. S3, available at http://www.jcb.org/cgi/content/full/jcb.200505071/DC1); note that a large pool of noncentrosomal γ-tubulin is found both in soluble and insoluble fractions in cells (Moudjou et al., 1996).

Our live imaging showed that microtubules on MDCK basal patches form intersections at the growing (plus) ends of microtubules with the sides of microtubules (Reilein and Nelson, 2005) as well as the minus end (origin of growth) and the sides of microtubules (Fig. 4, A and B, and see Fig. 8). Presumably, γ-tubulin is localizing to the minus end of the microtubule at branch points, although we cannot confirm this directly from the fixed images. We observed two different configurations of microtubule ends intersecting with the sides of microtubules by electron microscopy (Fig. 2). It is possible that these configurations could be plus and minus ends forming intersections with other microtubules, although other possibilities exist (for example, plus ends that are growing or pausing).

Whereas one end of the microtubules underwent periods of growth and shrinkage, which is indicative of the plus end, most of the newly arisen microtubules (19/26 observed in nine cytoplasts) showed shrinkage from the other end, which is designated the minus end (Fig. 4, A–C and E); minus end–shortening rates varied from 3 to 15 μm/min (Fig. 5). Our designation of the microtubule plus and minus ends based on their respective dynamics was independently confirmed by analyzing microtubule dynamics in basal cytoplasts from MDCK cells expressing the microtubule plus end marker protein EB1 tandem dimer (td) DsRed (Fig. 5 and Video 6, available at http://www.jcb.org/cgi/content/full/jcb.200505071/DC1). Note that EB1 bound along the entire length of microtubules but was enriched on the growing plus ends of microtubules (Reilein and Nelson, 2005). The bimodal distribution of EB1 movements (at the plus end of microtubules) is similar to that of unmarked microtubules, in which we identified the plus end as the rapidly growing end of the microtubule (Fig. 5, A and C). EB1 is also visible on microtubules undergoing dynamic instability at the edge of the cytoplast (Video 6). The behavior of the minus end of microtubules in these basal cytoplasts is different from that of acentrosomal microtubules in other epithelial cell types in which the minus end was reported to be stable (Vorobjev et al., 1997; Yvon and Wadsworth, 1997). Note, however, that depolymerizing minus ends often paused or became stabilized upon reaching another microtubule or area of stabilization on the cortex (Fig. 4).

In summary, we observed three major types of microtubule activities in the network: (1) stably localized microtubules, (2) microtubules undergoing dynamic instability at one end and, in some cases, shrinking from the other end, and (3) microtubules arising de novo and integrating into the network. These parameters generate a network that appears to have an overall steady-state pattern and yet has intrinsic dynamic properties that cause some remodeling of the pattern over time.

Computational modeling of microtubule parameters required for the formation of a steady-state microtubule network

The apparent random organization of microtubules in the basal network might suggest that the network could arise by the simple overlap of microtubules undergoing dynamic instability. However, our analysis of the network in situ revealed that additional parameters were involved, including increased microtubule stabilization as a result of microtubule–cortex and microtubule–microtubule interactions. To test the requirement of different microtubule parameters on the formation of the network, we developed a computational model that simulated dynamic microtubules in a two-dimensional space (see Materials and methods). Our goal was to define a minimal set of parameters that are necessary and sufficient to form a steady-state microtubule network.

We first tested whether the simulated assembly of 30 microtubules undergoing dynamic instability as the only parameter could lead to the formation of a steady-state structure. In this test, one end of the microtubule was modeled to undergo dynamic instability (designated the plus end), whereas the other end was kept inert (designated the minus end). This simulation resulted in a distribution of microtubules (mean length 2.3 ± 0.4 μm) in a 5 × 5–μm space that exhibited continuous remodeling as a result of the disappearance of microtubules by depolymerization and spontaneous nucleation of microtubules elsewhere at random in the space (Fig. 7 A).

To simulate microtubule stabilization as observed in situ, the rescue frequency was arbitrarily increased to a 50% chance of being rescued per second (30-fold over the experimentally measured value) when microtubule plus ends encountered other microtubules (Fig. 7 A, MT–MT) or 100-nm spots (n = 200) randomly placed to mimic the distribution of APC (Fig. 7 A, MT–cortex); that is, when a growing or shrinking microtubule encountered either of these stabilization points, it was prevented from depolymerizing (Fig. 7 A) as shown in situ (Fig. 4; Reilein and Nelson, 2005). Because of these stabilization events, the mean length of microtubules increased to 2.8 ± 0.2 μm in the case when only microtubule–microtubule interactions were used in the simulation and to 2.9 ± 0.2 μm when only microtubule–cortex interactions were used (Fig. 7 B).

To measure the development of the network, individual time frames were correlated with future frames (Δt = 2 min; for a rationale for choosing this time interval, see Fig. S1, available at http://www.jcb.org/cgi/content/full/jcb.200505071/DC1). To determine to what degree a stable configuration had been

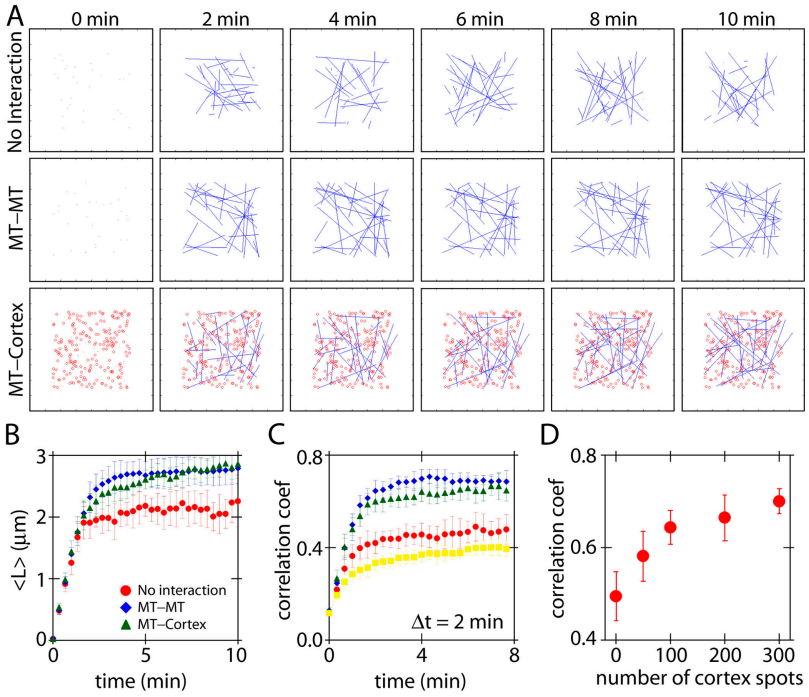

Figure 7. **Stochastic simulation of microtubule network formation.** (A) Simulated microtubule dynamics with or without plus end stabilization. Stabilization was simulated by an increase in rescue frequency when the plus end encountered another microtubule (MT–MT) or randomly distributed cortical spots (MT–cortex). Microtubules form a steady-state pattern in the presence of either microtubule–microtubule or microtubule–cortex interactions. Blue lines represent microtubules; red circles represent cortical stabilization points. See Videos 7 and 8 (available at http://www.jcb.org/cgi/content/full/jcb.200505071/DC1). (B) The mean lengths of microtubules in each simulation (n = 10 simulations). (C) Formation of steady-state networks was measured by the correlation between two time steps separated by Δt = 2 min (see Materials and methods for details). Symbols are the same as in B. Background correlation coefficients (squares) were calculated between two unrelated simulations. Correlation coefficients are highest for simulated microtubule networks with stabilization points. (D) The effect of increasing the number of cortical stabilization points on the correlation coefficient. Δt = 2 min. Error bars represent SD.

generated, we used the correlation coefficient as an index to compare how well two images align with one another. Image correlation analysis is used frequently to compare two images for pattern similarity, such as in fingerprint matching (Russ, 1998). The correlation coefficient is zero when two images are dissimilar and is one when two images are identical. Therefore, we defined a network as being at steady state when it reached and maintained a high correlation coefficient. Such a network contains a microtubule pattern that does not undergo large changes but has some slow remodeling as a result of dynamic instability at the plus end of some microtubules and the de novo growth and depolymerization of a relatively minor fraction of microtubules. A self-organizing system must be continually dynamic yet maintain a stable pattern, and, therefore, the correlation coefficient should be high but should not reach one (Misteli, 2001; Anderson, 2002).

We simulated microtubule network formation for three conditions: no interactions, microtubule–microtubule stabilization, and microtubule–cortex stabilization. In all conditions, the correlation coefficient and microtubule length increased at similar rates and reached steady state (Fig. 7 B). In the case with no interactions, the microtubules reached a steady-state length but not a steady-state pattern; consequently, the correlation coefficient was low. However, the highest correlation coefficients occurred in networks formed with either microtubule–microtubule or microtubule–cortex stabilization points (Fig. 7 C). We also examined the effect of increasing the number of cortex stabilization points on the correlation coefficient for network formation (Fig. 7 D). Fig. 7 D shows that the correlation increases with an increasing number of cortical stabilization points. Thus, in the simulation, microtubule–microtubule and microtubule–cortex stabilization can cause the formation of a steady-state microtubule network. Together, these in situ and in silico analyses indicate that the stabilization of microtubules either by microtubule–microtubule or microtubule–cortex interactions can cause the formation of a steady-state network. In situ, the cortical interactions help to maintain the location of stable microtubules.

As a further test of the computational model, we sought to examine the formation of a microtubule network in silico using the locations of cortical stabilization spots and microtubule nucleation sites taken from an in situ example and the aforementioned microtubule stabilization criteria. Fortuitously, we imaged a basal cytoplast that spontaneously assembled a de novo microtubule network in ~10 min after a lag of ~9 min, which could be used for this direct comparison (Fig. 8). The reason for this lag is unknown, but it is inconsequential for the comparative analysis of in situ and in silico growth of the network. Note that this type of naked patch was a rare event; this patch had probably lost most of its microtubules during sonication and, therefore, had a large surface of APC spots over which a new microtubule network could form. Nevertheless, this patch, albeit rare, was very useful as it allowed us to test our simulation under more stringent conditions of almost complete de novo formation of a microtubule network. A similar analysis was also performed on a patch with a less dramatic reorganization of the microtubule network (Fig. S2, available at http://www.jcb.org/cgi/content/full/jcb.200505071/DC1). Microtubules grew from the sides or ends or other microtubules and integrated into the forming network through connections with other microtubules (Fig. 8 and Video 9, available at http://www.jcb.org/cgi/content/full/jcb.200505071/DC1). The network appeared to reach a steady state that persisted for the additional 20 min of imaging. Retrospective staining for APC showed that many of the microtubules had grown over and remained colocalized with APC spots on the cortex (Fig. 9 A) as

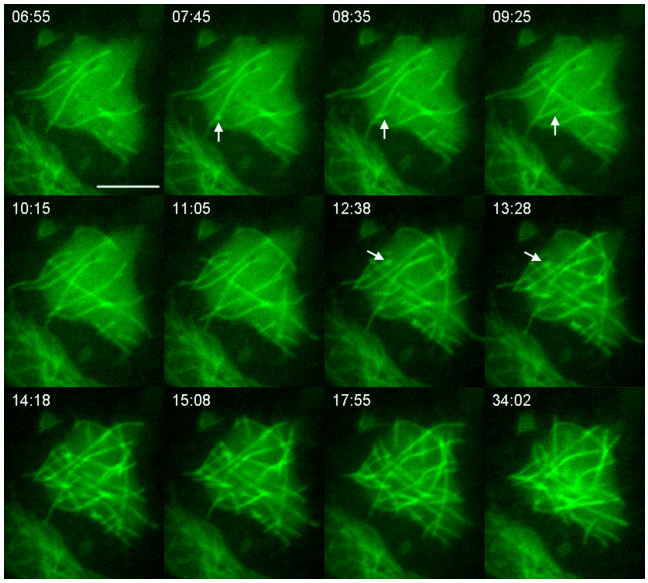

Figure 8. **Assembly of the microtubule network in a basal cytoplast.** In a basal cytoplast that had only a few microtubules remaining after sonication, microtubules assembled into a steady-state network in ~10 min. The network had a similar appearance 15 min after the assembly (compare the last two panels), indicating that it had reached a steady state. Arrows indicate examples of microtubules arising from the sides of other microtubules. Bar, 5 μm.

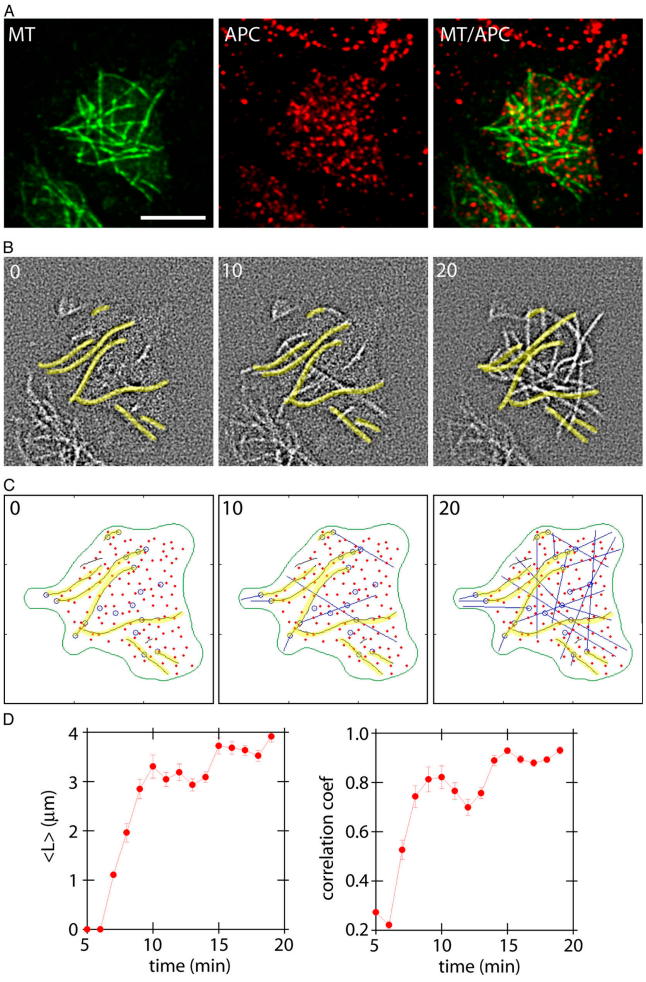

Figure 9. **Stochastic simulation based on an in situ microtubule network.** (A) Retrospective staining of APC for the microtubule network shown in Fig. 8. The location of the APC spots are used in the simulation below. Bar, 5 μm. (B) Although new microtubules added to the network, the original microtubules remained in place (marked in yellow). Time is given in minutes. (C) Stochastic simulation based on the in situ patch. Yellow filaments are preexisting microtubules; red dots are APC spots derived from the retrospective image; blue circles are nucleation sites derived from the in situ patch; blue lines represent microtubules. (D) The mean lengths of newly added microtubules and correlation coefficients of the simulated microtubule network. The curve levels off at a high correlation at 15 min, indicating that the network has reached a steady state. Error bars represent SD.

shown previously (Reilein and Nelson, 2005). Fig. 9 B shows still images from Video 9 using the microtubules from t = 0 min as fiduciary marks. To generate an in silico model of this microtubule network, we first mapped the boundary of the basal cytoplast, the distributions of APC spots and the original microtubules (t = 0 min), and the relative positions of all microtubule nucleation events that occurred (Fig. 9 C). We then let the simulation run using the parameter of increased rescue frequency upon microtubule–microtubule and microtubule–cortex (APC spots) interactions (Fig. 9 C). The pattern of microtubules that arose appears to be similar to that of the in situ microtubule network at 20 min. Further analysis showed that the mean length of microtubules in silico increased rapidly to 3.9 ± 2.4 μm (Fig. 9 D), which is comparable with the in situ mean length of 3.6 ± 2.0 μm. Although there were some fluctuations in the correlation coefficient as a result of the irregular timing of nucleation events that added new microtubules to the pattern, it reached a plateau approaching a correlation coefficient of one (Fig. 9 D), which is demonstrative of a steady-state microtubule network.

Our computational modeling demonstrates that randomly generated microtubule nucleation sites coupled with microtubule stabilization upon microtubule–microtubule and microtubule–cortex interactions can reconstitute a steady-state microtubule network. Moreover, using experimentally defined microtubule nucleation sites and microtubule–cortex interaction sites, the model can faithfully generate a steady-state microtubule network that is closely similar to one formed in situ. The final pattern is determined by the sites of nucleation and the location of cortical stabilization points (APC puncta). Thus, we have defined a minimal set of parameters from which an overall stable configuration of microtubules can be generated from dynamic components, which is the definition of a self-organizing structure (Misteli, 2001).

Discussion

Microtubules have distinctive distributions in cells, including arrays that emanate from the centrosome in interphase cells, radial asters that form the spindle in mitosis, and bundles of acentrosomal microtubules such as those found in neurons, muscle cells, and at the plant cell cortex. An important question is how cells generate these different microtubule organizations using well-defined properties of dynamic instability, plus and minus end–directed motor proteins, and microtubule-associated proteins (for review see Keating and Borisy, 1999). The radial ar-

ray of microtubules in the mitotic spindle is primarily organized by plus and minus end–directed microtubule motor proteins (Sawin et al., 1992; Nedelec et al., 1997; Surrey et al., 2001). Computational modeling indicates that the minus end–directed motor dynein on pigment granules is sufficient to organize a microtubule radial array (Vorobjev et al., 2001; Cytrynbaum et al., 2004; Malikov et al., 2004). Cortical microtubule arrays in plants are generated from randomly nucleated microtubules that at first are disorganized, but through treadmilling and dynamic instability, arrange themselves into parallel bundles that form helical microtubule arrays bound to the cortex (Shaw et al., 2003; Dixit and Cyr, 2004a,b).

In this study, we report the organization of microtubule networks bound to the basal cortex of polarized epithelial cells. These microtubules form the base of microtubule bundles that span the apico–basal axis of these columnar cells and, as we showed, are active in the transport of endocytic vesicles on the basal membrane. The organizational cues for this cortical microtubule network do not appear to involve treadmilling or motor proteins. Treadmilling gives the appearance of microtubule translocation as a result of the simultaneous addition of tubulin subunits to the plus end and subtraction from the minus end; this behavior was not observed in the basal cytoplasts. We also found little evidence for the involvement of microtubule motors in network organization on the basal membrane. It is noteworthy that the network does contain both plus and minus end–directed motor activity as evidenced by the bidirectional movement of endocytic vesicles over the microtubules at rates comparable to those of kinesins and dynein. However, we did not observe microtubules gliding on the surface of the basal cortex. We occasionally observed a microtubule tip sliding along another microtubule, but in those few cases, the rates of movement were slower than that expected of kinesins and dynein and were more consistent with microtubule polymerization.

Instead, our results indicate that the basal microtubule network is generated by increased microtubule stabilization at sites of microtubule–microtubule and microtubule–cortex intersections. Which proteins contribute to these stabilization points? We have shown previously that +Tip proteins APC, EB1, and $p150^{Glued}$ in the basal network are distributed not just at the plus ends of microtubules but along the length of microtubules and that they localize to the end of one microtubule binding to the side of another (Reilein and Nelson, 2005). We also showed that γ-tubulin was localized along microtubules, at intersections between two microtubules, and, possibly, between microtubules and the cortex; these observations are similar to recent results on the distribution of γ-tubulin along microtubules and in the cytoplasm of other cells (Janson et al., 2005; Murata et al., 2005). In addition, APC and perhaps other proteins associated with the basal cortex form a template for organization and polymerization of microtubules. We showed that microtubules pause and shrink to small stubs at distinct points on the membrane cortex without completely depolymerizing, which is indicative of points of microtubule stabilization on the basal cortex (Reilein and Nelson, 2005). Moreover, purified tubulin dimers assembled into microtubule networks over these APC spots on the cortex that were similar in organization and complexity to that in intact cells and on isolated basal membrane patches. Significantly, antibodies to APC inhibited the formation of this network (Reilein and Nelson, 2005), indicating a direct role of APC in binding and stabilizing polymerizing microtubules.

We tested whether a stable microtubule network can be formed in silico by superimposing dynamic instability with only the additional parameters of increased microtubule rescue frequency associated with microtubule–microtubule and microtubule–cortex binding, as we observed in situ. By direct comparison with a microtubule network formed in situ, we found that our in silico model of microtubule network assembly using a minimum of microtubule parameters faithfully reproduces the assembly and dynamic organization of a bone fide basal microtubule network. Both the in silico and in situ microtubule networks assembled from microtubules that continued to display dynamic instability and add and subtract microtubules from the network and yet maintained the same overall pattern, indicating that they had reached a steady-state organization. The simulation illustrates the minimal parameters that are involved in remodeling the network in situ. However, it is likely that other parameters play a role: for example, depolymerization of the minus ends contributes to the ability of the microtubule network to remodel itself after reaching an overall steady-state pattern. This parameter was not included in the computational model, as the timing of minus end depolymerization could not be predicted.

A self-organizing structure is defined as a dynamic structure in which material must be continuously exchanged but has an overall stable configuration (Misteli, 2001), and the emergence of a structure that arises from multiple local interactions in which the global level organization must arise solely from within the system and must not be generated from external guiding forces (Anderson, 2002). Thus, our analysis of microtubule networks on the basal cortex of polarized cells has uncovered a new mechanism for the self-organization of microtubules undergoing dynamic instability that requires increased microtubule stabilization associated with microtubule–microtubule and microtubule–cortex binding.

Materials and methods

Cell lines and transfection

The MDCK GFP-tubulin cell line (constructed by Angela Barth [Stanford University, Stanford, CA] and Eugenio de Hostos [Cytokinetics, South San Francisco, CA]) was made by inserting human α-tubulin into MDCK II cells. The MDCK EB1-td DsRed cell line was constructed by Angela Barth and Ryan Louie (Stanford University, Stanford, CA). MDCK type II/G cells were grown in DME supplemented with 10% FBS. EpH4 mouse mammary gland epithelial cells (Reichmann et al., 1989) were grown in DME–high glucose supplemented with 5% FBS and 10 mM Hepes. The Caco-2 "brush border-expressing" human colon adenocarinoma cell line C2BBE1 was obtained from the American Type Culture Collection and was grown in DME without phenol red and supplemented with 4.5 g L-glucose, 1.5 g L-sodium bicarbonate, 0.01 mg/ml human transferrin, and 10% FBS. For expression of clathrin-DsRed (a gift of Tomas Kirchhausen, Harvard Medical School, Cambridge, MA), cells were simultaneously transfected and seeded onto transwell filters at confluent density. 0.5 μg plasmid DNA per 12-mm filter was transfected using LipofectAMINE 2000 (Invitrogen) by mixing with 7×10^5 cells/filter; cells were allowed to polarize for 3–5 d before the preparation of basal cytoplasts. For experiments with LysoTracker red (Invitrogen), polarized cells on filters were incubated with 75 nM LysoTracker for at least 2 h before the preparation of basal cytoplasts.

Basal membrane isolation

Cells were plated at confluent density on 12-mm transwell polycarbonate filter membranes of 0.4-μm pore size (Corning) and were grown for 3–5 d (MDCK and EpH4 cells) or 2 wk (Caco-2 cells) to allow for cell polarization. Cells were rinsed and incubated for 10 min in hypotonic buffer (15 mM Hepes, pH 7.3, 15 mM KCl, 1 mM $MgCl_2$, and 1 mM EGTA) and sonicated at 4°C with a brief (<1 s) pulse using a sonifier (model 250; Branson Ultrasonics) set at duty cycle 20 and an output 19–22% with a 1/8-inch microprobe held ~5–7 mm above the surface of the cells (Drees et al., 2005). Membrane patches were rinsed briefly in buffer before imaging or fixation.

Fixation and antibodies

Fixation of microtubules in fully polarized cells on filters was performed with 0.3% glutaraldehyde and 0.1% Triton X-100 in 37°C BRB80 buffer (80 mM Pipes, pH 6.9, 1 mM EGTA, and 1 mM $MgCl_2$) for 20 min with gentle agitation followed by three 5-min washes in 1 mg/ml $NaBH_4$ in Ringers buffer to quench unreacted aldehyde groups. The fixation of microtubules on isolated membrane patches was performed with 0.3% glutaraldehyde except in the case of γ-tubulin staining, in which basal patches were fixed with 0.08% glutaraldehyde and 2% freshly prepared PFA in BRB80, as suggested by Murata et al. (2005). Microtubules were stained with DM1A mouse monoclonal α-tubulin antibody (Sigma-Aldrich), γ-tubulin was stained with mouse monoclonal GTU-88 (Sigma-Aldrich), and APC was stained with an affinity-purified polyclonal antibody to a central APC2 domain (Munemitsu et al., 1994). Secondary antibodies conjugated to FITC or rhodamine were obtained from Jackson ImmunoResearch Laboratories. Specimens were mounted in Vectashield mounting medium (Vector Laboratories).

Fluorescence microscopy of fixed specimens

Image z-stacks were collected in 0.20-μm steps on an inverted microscope (IX-70; Olympus) with a 100× NA 1.35 oil immersion objective (Olympus) and were captured with a cooled CCD camera (Photometrics). Images were collected at room temperature and processed using DeltaVision deconvolution software (Applied Precision) on a workstation (Silicon Graphics, Inc.). For three-dimensional image reconstruction, deconvolved optical sections were combined using Volocity software (Improvision, Inc.).

Scanning electron microscopy

Basal membranes were prepared from MDCK cells polarized on transwell filters and were fixed for 30 min in 2% glutaraldehdye in BRB80 buffer. For gold labeling of microtubules, unreacted aldehydes were quenched with $NaBH_4$, and microtubules were stained with the DM1A monoclonal antibody diluted 1:50 followed by 15 nm gold-labeled secondary antibody. Samples were fixed again after immunolabeling in 2% glutaraldehyde. Samples were processed according to the procedure of Svitkina et al. (1995). In brief, samples were changed from glutaraldehyde to 0.1% tannic acid for 20 min and 0.1% uranyl acetate for 20 min, dehydrated through an ethanol series, and critical point dried in ethanol. Filters were cut from the plastic holders only after critical point drying. Samples were rotary shadowed with platinum at a 45° angle. Samples were imaged with a scanning electron microscope (XL30 Sirion; FEI Company) at 5 kV and spot size 3 in ultrahigh resolution mode.

Live imaging of basal cytoplasts

MDCK cells were plated at confluent density on transwell filters and grown 3–5 d to allow for cell polarization. Basal membranes were prepared as described above. Filters were rinsed several times in BRB80 buffer, mounted on a glass slide between two strips of double-stick tape, and covered with BRB80 buffer with 2 mM ATP and 1 mM GTP. A 22-mm glass coverslip was placed on top and sealed in place with silicone vacuum grease. The inclusion of 2 mM ATP and 1 mM GTP in the sonication and imaging buffers resulted in similar parameters of microtubule dynamics and vesicle motility as those without these nucleotides added, indicating that cytoplasts sealed over very quickly after sonication. Basal patches that exhibited microtubule dynamics were presumed to be sealed-over cytoplasts. Fluorescence imaging was performed with a microscope (200M Axiovert; Carl Zeiss MicroImaging, Inc.) run by Slidebook software (Marianas System; Intelligent Imaging Innovation, Inc.) using a 100× NA 1.4 objective lens heated to 37°C. For imaging of EB1-td DsRed or of microtubule dynamics with GFP-tubulin, images were captured for 5 s each with no interval between frames. For imaging of vesicles moving along microtubules, LysoTracker red was imaged with a DsRed filter for 200 ms or clathrin-DsRed for 3 s, and GFP-tubulin was imaged with the GFP filter for 4 s. Retrospective staining of APC was performed as described previously (Reilein and Nelson, 2005).

Analysis of microtubule dynamics

Images were sharpened in ImageJ (National Institutes of Health) with the Fourier transform bandpass filter to remove high and low spatial frequency signals using the limits of 0.192–1.6 μm. The positions of plus or minus ends of individual microtubules with time were measured in ImageJ and exported to Microsoft Excel. The lengths of individual microtubules were graphed as a function of time (life histories). Only microtubules that were actively undergoing growth and shrinkage were followed, not the microtubules that were in an extended state of pause. The rates of growth and shortening events were determined by linear regression of events with changes in length ≥0.7 μm. Means and SDs were calculated per event. The catastrophe frequency was calculated by dividing the number of transitions from growth or pause to shortening by the total time for each individual microtubule. The rescue frequency was calculated by dividing the total number of transitions from shortening to pause or growth by the total time for each individual microtubule. Changes in length of <0.15 μm were considered to be pauses.

Stochastic simulation of microtubule dynamics

Computer-simulated microtubules diffusing and exhibiting dynamic instability at their plus ends were nucleated randomly in a 5 × 5–μm space. If a microtubule depolymerized completely, a new nucleation site was assigned randomly. The dynamic instability was simulated with catastrophe (= 0.003 × L) and rescue (= 0.003 × [13-L]) frequency (1/s), where L is microtubule length (Nedelec, 2002). Experimentally measured growth (2.54 μm/min) and shrinkage (5.06 μm/min) rates were used for the simulation. Drag coefficients for translational and rotational diffusion are microtubule length dependent (Howard, 2001) and were calculated using a fluid viscosity of 0.05 $pNs/\mu m^2$ (Nedelec, 2002). To prevent microtubules from growing beyond the boundary, the catastrophe frequency was increased when microtubule tips exceeded the boundary. A point of stabilization in the microtubule network was modeled as an increase in the rescue frequency to 0.5/s when the tip was within 50 nm of the stabilization spot. All calculations were performed using Matlab (Mathworks).

We compared the distribution of microtubules in two images of a simulated microtubule network separated by Δt. The image correlation analysis is used frequently to compare two images for pattern similarity (Russ, 1998). The correlation coefficient is zero when two images are dissimilar and is one when two images are identical. Correlation coefficients are calculated by performing conjugate multiplication in the Fourier domain using Matlab; Δt = 2 min was chosen as the time interval based on the graph in Fig. S1. The correlation coefficient is defined as the maximum value of inverted Fourier transformed images. This image correlation does not recognize individual microtubules but rather recognizes the overall image pattern of the simulated microtubule network. Thus, the correlation depends on the differences in the pattern and density of the network from one time point to another. As a result, the correlation between two independent simulations will have a background correlation value (Fig. 7 C, squares). The correlation coefficient was calculated over the time course with a fixed time interval (Δt = 2 min; Fig. 7 C).

For the simulation based on the in situ patch in Fig. 8, the coordinates of preexisting microtubules, nucleation sites, the direction of polymerization, and the cortex interaction sites were taken from the patch shown in Figs. 8 and 9 A. A similar analysis was performed for the patch shown in Fig. S2.

Online supplemental material

Fig. S1 shows the relationship of the correlation coefficient to Δt. Fig. S2 shows a second example of a computational analysis based on an in situ microtubule network. Fig. S3 shows centrosomal and noncentrosomal γ-tubulin staining in whole MDCK cells. Video 1 shows LysoTracker red–labeled vesicles moving along microtubules in a basal cytoplast. Video 2 shows clathrin-DsRed–labeled vesicles moving on microtubules in a basal cytoplast. Video 3 shows microtubules arising de novo from the sides of other microtubules in an MDCK cell basal cytoplast. Video 4 shows microtubules in an MDCK cell basal cytoplast slowing and pausing at points on the cortex. Video 5 shows a de novo microtubule growing over a specific point where another microtubule end terminates in an MDCK cell basal cytoplast. Video 6 shows a basal cytoplast prepared from polarized cells expressing EB1-td DsRed. Video 7 shows computer-generated images of simulated microtubule networks with no microtubule interactions and microtubule–microtubule interactions. Video 8 is a simulation of a microtubule network with microtubule–cortex interactions. Video 9 shows the de novo formation of a microtubule network in a basal cytoplast. Video 10 is a computer simulation based on the in situ microtubule network shown in Video 9. Online supplemental material is available at http://www.jcb.org/cgi/content/full/jcb.200505071/DC1.

We would like to thank John Perrino and Jon Mulholland for help with electron microscopy and Vladimir Rodinov and Vladimir Gelfand for comments on an early version of the manuscript.

This work was supported by a National Cancer Institute grant (PHS 5T32CA09151) to A. Reilein, the Department of Health and Human Services, an American Cancer Society Postdoctoral Fellowship grant (PF-03-016-01-CSM) to A. Reilein, and a National Institutes of Health grant (GM35527) to W.J. Nelson.

Submitted: 12 May 2005
Accepted: 27 October 2005

References

Anderson, C. 2002. Self-organization in relation to several similar concepts: are the boundaries to self-organization indistinct? *Biol. Bull.* 202:247–255.

Bacallao, R., C. Antony, C. Dotti, E. Karsenti, E.H. Stelzer, and K. Simons. 1989. The subcellular organization of Madin-Darby canine kidney cells during the formation of a polarized epithelium. *J. Cell Biol.* 109:2817–2832.

Bre, M.H., T.E. Kreis, and E. Karsenti. 1987. Control of microtubule nucleation and stability in Madin-Darby canine kidney cells: the occurrence of noncentrosomal, stable detyrosinated microtubules. *J. Cell Biol.* 105:1283–1296.

Chausovsky, A., A.D. Bershadsky, and G.G. Borisy. 2000. Cadherin-mediated regulation of microtubule dynamics. *Nat. Cell Biol.* 2:797–804.

Cytrynbaum, E.N., V. Rodionov, and A. Mogilner. 2004. Computational model of dynein-dependent self-organization of microtubule asters. *J. Cell Sci.* 117:1381–1397.

Dixit, R., and R. Cyr. 2004a. The cortical microtubule array: from dynamics to organization. *Plant Cell.* 16:2546–2552.

Dixit, R., and R. Cyr. 2004b. Encounters between dynamic cortical microtubules promote ordering of the cortical array through angle-dependent modifications of microtubule behavior. *Plant Cell.* 16:3274–3284.

Drees, F., A. Reilein, and W.J. Nelson. 2005. Cell-adhesion assays: fabrication of an e-cadherin substratum and isolation of lateral and Basal membrane patches. *Methods Mol. Biol.* 294:303–320.

Eaton, S., R. Wepf, and K. Simons. 1996. Roles for Rac1 and Cdc42 in planar polarization and hair outgrowth in the wing of *Drosophila*. *J. Cell Biol.* 135:1277–1289.

Gilbert, T., A. Le Bivic, A. Quaroni, and E. Rodriguez-Boulan. 1991. Microtubular organization and its involvement in the biogenetic pathways of plasma membrane proteins in Caco-2 intestinal epithelial cells. *J. Cell Biol.* 113:275–288.

Heuser, J. 2000. The production of 'cell cortices' for light and electron microscopy. *Traffic.* 1:545–552.

Howard, J. 2001. Mechanics of Motor Proteins and the Cytoskeleton. Sinauer Associates, Inc., Sunderland, MA. 367 pp.

Janson, M.E., T.G. Setty, A. Paoletti, and P.T. Tran. 2005. Efficient formation of bipolar microtubule bundles requires microtubule-bound γ-tubulin complexes. *J. Cell Biol.* 169:297–308.

Keating, T.J., and G.G. Borisy. 1999. Centrosomal and non-centrosomal microtubules. *Biol. Cell.* 91:321–329.

Keyel, P.A., S.C. Watkins, and L.M. Traub. 2004. Endocytic adaptor molecules reveal an endosomal population of clathrin by total internal reflection fluorescence microscopy. *J. Biol. Chem.* 279:13190–13204.

Komarova, Y.A., I.A. Vorobjev, and G.G. Borisy. 2002. Life cycle of MTs: persistent growth in the cell interior, asymmetric transition frequencies and effects of the cell boundary. *J. Cell Sci.* 115:3527–3539.

Malikov, V., A. Kashina, and V. Rodionov. 2004. Cytoplasmic dynein nucleates microtubules to organize them into radial arrays in vivo. *Mol. Biol. Cell.* 15:2742–2749.

Meads, T., and T.A. Schroer. 1995. Polarity and nucleation of microtubules in polarized epithelial cells. *Cell Motil. Cytoskeleton.* 32:273–288.

Misteli, T. 2001. The concept of self-organization in cellular architecture. *J. Cell Biol.* 155:181–185.

Mitchison, T., and M. Kirschner. 1984. Dynamic instability of microtubule growth. *Nature.* 312:237–242.

Moudjou, M., N. Bordes, M. Paintrand, and M. Bornens. 1996. γ-Tubulin in mammalian cells: the centrosomal and the cytosolic forms. *J. Cell Sci.* 109:875–887.

Munemitsu, S., B. Souza, O. Muller, I. Albert, B. Rubinfeld, and P. Polakis. 1994. The APC gene product associates with microtubules in vivo and promotes their assembly in vitro. *Cancer Res.* 54:3676–3681.

Murata, T., S. Sonobe, T.I. Baskin, S. Hyodo, S. Hasezawa, T. Nagata, T. Horio, and M. Hasebe. 2005. Microtubule-dependent microtubule nucleation based on recruitment of gamma-tubulin in higher plants. *Nat. Cell Biol.* 7:961–968.

Nedelec, F. 2002. Computer simulations reveal motor properties generating stable antiparallel microtubule interactions. *J. Cell Biol.* 158:1005–1015.

Nedelec, F.J., T. Surrey, A.C. Maggs, and S. Leibler. 1997. Self-organization of microtubules and motors. *Nature.* 389:305–308.

Pepperkok, R., M.H. Bre, J. Davoust, and T.E. Kreis. 1990. Microtubules are stabilized in confluent epithelial cells but not in fibroblasts. *J. Cell Biol.* 111:3003–3012.

Perret, E., A. Lakkaraju, S. Deborde, R. Schreiner, and E. Rodriguez-Boulan. 2005. Evolving endosomes: how many varieties and why? *Curr. Opin. Cell Biol.* 17:423–434.

Rappoport, J.Z., B.W. Taha, and S.M. Simon. 2003. Movement of plasma-membrane-associated clathrin spots along the microtubule cytoskeleton. *Traffic.* 4:460–467.

Reichmann, E., R. Ball, B. Groner, and R.R. Friis. 1989. New mammary epithelial and fibroblastic cell clones in coculture form structures competent to differentiate functionally. *J. Cell Biol.* 108:1127–1138.

Reilein, A., and W.J. Nelson. 2005. APC is a component of an organizing template for cortical microtubule networks. *Nat. Cell Biol.* 7:463–473.

Rodionov, V., E. Nadezhdina, and G. Borisy. 1999. Centrosomal control of microtubule dynamics. *Proc. Natl. Acad. Sci. USA.* 96:115–120.

Russ, J.C. 1998. The Image Processing Handbook. CRC Press, Boca Raton, FL. 771 pp.

Sawin, K.E., K. LeGuellec, M. Philippe, and T.J. Mitchison. 1992. Mitotic spindle organization by a plus-end-directed microtubule motor. *Nature.* 359:540–543.

Shaw, S.L., R. Kamyar, and D.W. Ehrhardt. 2003. Sustained microtubule treadmilling in *Arabidopsis* cortical arrays. *Science.* 300:1715–1718.

Shelden, E., and P. Wadsworth. 1993. Observation and quantification of individual microtubule behavior in vivo: microtubule dynamics are cell-type specific. *J. Cell Biol.* 120:935–945.

Surrey, T., F. Nedelec, S. Leibler, and E. Karsenti. 2001. Physical properties determining self-organization of motors and microtubules. *Science.* 292:1167–1171.

Svitkina, T.M., A.B. Verkhovsky, and G.G. Borisy. 1995. Improved procedures for electron microscopic visualization of the cytoskeleton of cultured cells. *J. Struct. Biol.* 115:290–303.

Vorobjev, I., V. Malikov, and V. Rodionov. 2001. Self-organization of a radial microtubule array by dynein-dependent nucleation of microtubules. *Proc. Natl. Acad. Sci. USA.* 98:10160–10165.

Vorobjev, I.A., T.M. Svitkina, and G.G. Borisy. 1997. Cytoplasmic assembly of microtubules in cultured cells. *J. Cell Sci.* 110:2635–2645.

Waterman-Storer, C.M., W.C. Salmon, and E.D. Salmon. 2000. Feedback interactions between cell-cell adherens junctions and cytoskeletal dynamics in newt lung epithelial cells. *Mol. Biol. Cell.* 11:2471–2483.

Yvon, A.M., and P. Wadsworth. 1997. Non-centrosomal microtubule formation and measurement of minus end microtubule dynamics in A498 cells. *J. Cell Sci.* 110:2391–2401.